ELSEVIER

Contents lists available at ScienceDirect

Journal of Manufacturing Processes

journal homepage: www.elsevier.com/locate/manpro





Collaborative printing and in-situ frontal curing of highly-viscous thermosetting composites

Chongjie Gao^a, Ruochen Liu^b, Wei Li^a, Jingjing Qiu^c, Shiren Wang^{a,b,*}

- ^a Department of Industrial and Systems Engineering, Texas A&M University, College Station, TX 77843, USA
- ^b Department of Materials Science and Engineering, Texas A&M University, College Station, TX 77843, USA
- ^c Department of Mechanical Engineering, Texas A&M University, College Station, TX 77843, USA

ARTICLE INFO

Keywords: Collaborative printing Additive manufacturing Viscous resin Thermoset Frontal polymerization

ABSTRACT

Rapid manufacturing of thermosets via frontal polymerization is very attractive for thermosetting composites due to the expected decarbonization and manufacturing flexibility with limited energy consumption; however, it is challenging for 3D printing and frontal curing of highly-viscous thermoset composites (e.g., >100,000 mPa.s at room temperature) because of the rheology requirement of the 3D printing process and limited pot life of frontal curable resin inks under elevated temperature, which is usually used to reduce the viscosity of inks. We report an in-situ combining materials-based 3D printing process for printing and in-situ frontal curing of highly viscous thermosets. Specifically, an ultrasonic atomizer sprays the curing agent solution during the printing process to achieve an in-situ mixing with the resin oligomers at a microscale level. Multiphysics simulation indicated the curing degree distribution through the thickness direction and a printing window is provided depending on the extrusion deposition rate, the deposition layer thickness, and the ultrasonic sprayer amplitude. Further experiments were carried out, and it was found that the frontal velocity increased, and the frontal temperature remained almost unchanged with the rise of the ultrasonic amplitude. The curing degree and curing uniformity were improved with the increase of the ultrasonic amplitude but decreased with the increase of the printing layer thickness. Samples with different ultrasonic amplitudes and extrusion layer thicknesses were printed, and their mechanical properties were tested. The tensile strength and Young's modulus of novolac epoxy resin reached 47.56 MPa and 2.19 GPa, respectively. The feasibility of this method for composite printing was demonstrated. At a 5 wt% loading of short fibers, the tensile strength and Young's modulus of as-printed composites reached 66.71 MPa and 3.65 GPa. This method provides a fast and energy-efficient way to manufacture highly viscous thermosets and their composites.

1. Introduction

Molding, followed by thermal curing in an oven or autoclaves, is a standard fabrication method for high-performance thermosets, but it is energy-intensive, expensive, and time-consuming [1–5]. It was reported that the energy consumption for oven curing Boeing 787 fuselage made by thermoset-based composites is around 350 GJ, and the curing time takes over 8 h [6]. Therefore, the rapid manufacturing of thermosets with minimum energy consumption has received much attention from both the industry and academia [7–10]. Frontal polymerization is an exothermic reaction initiated by a small amount of heat. It leads to self-sustainable reaction waves without any external energy supply and is considered an energy-efficient curing method for thermosets

[1,8,11,12]. Frontal polymerization was integrated into additive manufacturing of thermosets by Robertson et al. in 2018 while frontal polymerization has been demonstrated since 1972 [13,14]. With this energy-efficient manufacturing method, Robertson et al. reported the fabrication of dicyclopentadiene (DCPD) and carbon fiber-reinforced DCPD. Zhang et al. investigated the catalytic effects of carbon-based nanomaterials on the frontal reaction during the additive manufacturing of epoxy. They concluded that carbon nanotubes (CNTs) and graphene oxide (GO) could reduce the activation energy of frontal polymerization significantly [15]. Uitz et al. developed a reactive extrusion system in which the resin and curing agents were stored in separate reservoirs and mixed during the printing to start the frontal polymerization. The tensile modulus and ultimate strength of printed

^{*} Corresponding author at: Department of Industrial and Systems Engineering, Texas A&M University, College Station, TX 77843, USA. *E-mail address:* s.wang@tamu.edu (S. Wang).

parts are isotropic [16].

In the previous reports, the frontal curable inks, which consist of monomers and initiators, were applied to achieve the in-situ curing integrated additive manufacturing of thermosets and their composites [17,18]. However, the reported printing process is only suitable for lowviscosity resin and is carried out at the ambient temperature or lowtemperature [18-20]. 3D printing of highly viscous resin with in-situ frontal curing remains a significant challenge because of the rheology requirement of the direct ink printing process. Another challenge is the dispersion of the frontal curing agents into the highly viscous resin since the common method of mixing the resin with curing agents is to dissolve the resin and curing agents into the solvent and evaporate the solvent or reduce the viscosity of the resin under elevated temperature and then mix with the curing agents. As a result, the pot life of frontal curable inks is very limited [18]. For example, mixing the curing agent with such viscous resins at 70 °C led to an extremely short pot life, <4 min, which does not allow to have sufficient time to load resins to the printer and print. Highly viscous thermosets, especially novolac epoxy, are recognized as a high-temperature resin widely applied in the flame retardancy, aerospace, and tooling industries, but the viscosity is extremely high, >100,000 mPa.s at 35 °C, making it difficult to be printed [21–23]. Daniel et al. reported a new additive manufacturing process that integrates direct ink writing (DIW) and vat photopolymerization (VP) to print highly viscous photoresins. Although the printing resolution is very high and polyimide photoresin with a viscosity of 770,000 mPa.s could be printed by their hybrid system, a post-thermal treatment process is required [24]. Gunduz et al. developed a direct ink-based additive manufacturing method using ultrasonic vibrations to manufacture heterogeneous materials for biomedical and structural applications [25]. The polymer clay material shows an extremely high viscosity (>100,000 mPa.s) and indicates difficult printability under room temperature. However, pure resin without fillers seems difficult to be printed out, and the printing resolution still remains a problem. Liu et al. created an acoustic liquefaction method to print ultrahigh-viscosity resin by enhancing the flow of yield stress fluids [26]. However, the printing system is very complex.

In this study, we demonstrated a collaborative printing method for highly-viscous resins by ultrasonic spraying of curing agents and extrusion deposition of thermosets and their composite inks to achieve in-situ mixing of resins and curing agents. The effect of the spraying amplitude and printing layer thickness on the frontal velocity and frontal temperature were studied. The curing degree and curing uniformity of printed samples were characterized. The tensile strength and Young's modulus of the printed samples were also analyzed. Besides, discontinuous carbon fibers (d-CF) and microballoons reinforced composites were manufactured by this novel printing method. The roles of the fillers in the composites were explored. The mechanical properties of the printed composites were characterized.

2. Materials and methods

2.1. Materials

DEN 438, a commercialized novolac epoxy resin, was purchased from Dow. 1,1,2,2–tetraphenyl-1,2–ethanediol (noted as I-TI) was purchased from Sigma Aldrich as the thermal initiator. Bis[4-(tert-butyl) phenyl] iodonium Tetra(nonflour-tert-butoxy) aluminate (noted as I-AI) was purchased from TCI as the cationic photoinitiator [27]. Acetone was purchased from Sigma Aldrich as the solvent. Phenolic microballoon (particle size: 5–127 μ m) and discontinuous carbon fiber (d-CFs, T800) with an average diameter of 8 μ m were kindly provided by the National Aeronautics and Space Administration (NASA). All the chemicals were used as received.

2.2. Ink and curing agent solution preparation

The pure thermoset inks were prepared directly by the pure novolac epoxy, and composites inks were formulated by adding 1 wt%, 3 wt%, 5 wt% d-CF, and 1 wt% glass microballoon as nanofillers. To prevent the agglomeration of nanofillers, the pure polymers were heated to 110 °C to ensure the fluidity of inks, and nanofillers were mixed with the heated inks by the magnetic stir. Then the mixtures were moved to the sonicator to enhance the dispersion of nanofillers for 24 h. A cylinder heater was submerged into the sink to heat water to ensure the temperature was at 85 °C. The curing agent solution was prepared by mixing I-AI and I-TI with a mole ratio of 2 to 0.1 in acetone.

2.3. Collaborative printing

The collaborative printing system consisted of three parts: a DIW 3D printer (Allevi 1), a syringe pump (Cole-Parmer EW-74900-85), and an ultrasonic atomizer (UCL120 with ultrasonic generator), as shown in Fig. 1 (a). The inks were loaded into a 5 mL syringe, and the extruder was heated to 65 °C to reduce the viscosity of the novolac epoxy resin. Molecular structures of the novolac epoxy and the initiators are illustrated in Fig. S1. The curing agent solution was loaded into a 2 mL syringe and placed on the syringe pump. One of the ultrasonic nozzle inlets was connected to the curing agent syringe by a plastic tube, and another was connected to the air gas pump to regulate the direction of the spraying droplets, as depicted in Fig. 1 (b). A strip heater (6'3", 180 W from Mcmaster-Carr) with a temperature controller (PM6L1AJ-AAAABBS from Watlow) was placed beneath the substrate as a heat supply. The 14-gauge needle was applied to print the resin with a selfequilibrating printing strategy [28]. The layer thicknesses were set to 0.05, 0.1, 0.25, and 0.5 mm. The flow rates of the curing agent solution were changed based on the printing thickness. The ultrasonic amplitudes were adjusted by the ultrasonic generator, and four amplitudes (0.01, 0.02, 0.04, 0.08) were tried for the printing process. The heating bed was set and kept at 90 °C to initiate frontal polymerization reaction and compensate for the heat dissipation caused by solvent evaporation during the printing process. The ultrasonic atomizer was opened 3 s before the printing to ensure the continuation of the spraying process. Fig. 1(c) shows the printed neat resin, d-CF thermoset composites, and microballon thermoset composites. The printed neat resin samples were numbered from S1 to S8, as shown in Table 1.

2.4. Characterization

2.4.1. Ultrasonic spraying process characterization

The diameters of the curing agent droplets were measured by an optical microscope (OLYMPUS, Model: BX51TRF). The sizes of the droplets were calculated by the software integrated with the microscope. The droplet size distribution was analyzed by ImageJ. At least 3 figures for each sample were analyzed, and average values were applied in this study.

2.4.2. Curing degree and curing uniformity

Differential scanning calorimetry (DSC, model: Q20, TA Instruments equipped with a CFL-50 cooling system) was applied to check the curing degree of novolac epoxy. 3–4 mg uncured resin specimens and 8–10 mg cured samples were obtained randomly and weighed in aluminum hermetic pans and heated from 50 to 235 °C with a heating rate of 10 °C $\,$ min $^{-1}$. The curing degree was calculated by the following equation [29]:

$$\alpha = \left\lceil 1 - \left(\frac{Hr}{Ht}\right) \right\rceil \times 100\%$$

where H_r is the heat of the reaction, H_t is the residual heat of the reaction [28]. At least 5 DSC data from the same sample were applied to obtain the standard derivation (SD) of the curing degree to analyze the curing

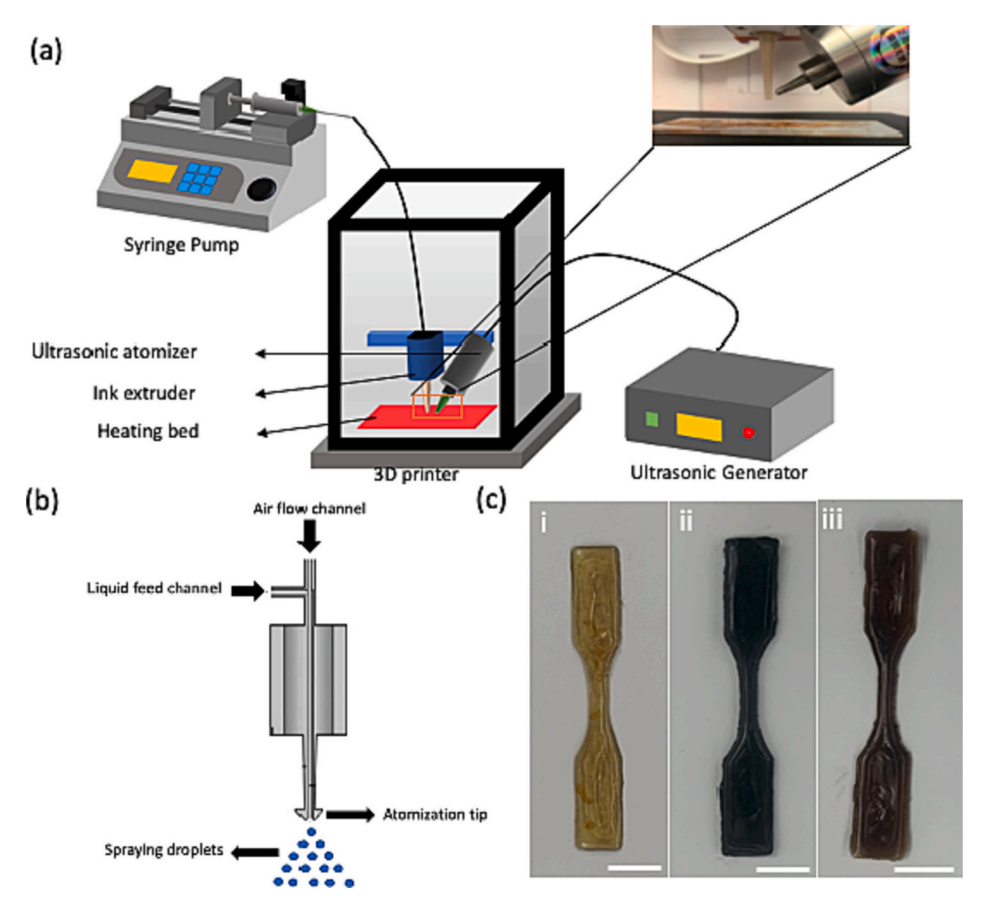


Fig. 1. (a) Schematic of collaborative printing of highly-viscous thermosets with concurrent extrusion deposition of resins and ultrasonic spraying of curing agent, (b) Schematic of ultrasonic atomizer for curing agent solution, (c) The printed tensile bars of neat thermosets and their composites (i: neat novolac epoxy, ii: d-CF novolac epoxy composites, iii: microballoon novolac epoxy composites, Scale bar: 10 mm, all the samples were printed under ultrasonic amplitude of 0.08 and layer thickness of 0.1 mm).

Table 1Printed neat resin samples.

Sample number	Ultrasonic amplitude	Layer thickness (mm)	Sample number	Ultrasonic amplitude	Layer thickness (mm)
S1	0.01	0.1	S5	0.08	0.05
S2	0.02	0.1	S6	0.08	0.1
S3	0.04	0.1	S7	0.08	0.25
S4	0.08	0.1	S8	0.08	0.5

variation caused by different amplitudes and printing layer thicknesses.

2.4.3. Mechanical property testing

The tensile test specimens were prepared according to ASTM 638 Type V, and then tested by Instron 3345 tensile machine (Instron Corporation, MA, USA) with a 2 kN load cell. The cross-section area of the samples was measured before the tests, and the tensile test speed was set to $10~\mathrm{mm}~\mathrm{min}^{-1}$. The tensile bar was gripped with sandpaper to increase the friction between the sample and the grip. The tensile strength and Young's modulus can be derived through the strain-stress curve. All specimens were tested after 3D printing without any post-treatment. All the measurements were conducted 3 times for each data point in this study. As a control, oven-cured samples were manufactured by the traditional molding method.

2.4.4. Rheological, frontal temperature, and velocity characterization

The rheology behaviors of the neat resin and composite inks were characterized by Anton Paar Physica MCR-301 rheometer. The infrared (IR) camera from FLIR (Model: A325sc) was used to record the temperature during the frontal polymerization. The frontal velocity was calculated from the distance traveled by the frontal wave. The IR camera

was calibrated by the procedures in the literature [29].

2.4.5. Numerical simulation

A numerical simulation was conducted to reveal the curing process along the thickness direction. The curing degree among the thickness direction was predicted to guide the layer thickness selection for 3D printing. The model layer number was set to 5 with a single layer thickness of 0.1 mm. A reactivity gradient was established based on the thickness. The behavior of the frontal wave was described by coupling of thermal diffusion and Arrhenius reaction kinetics [31,32]. The frontal polymerization could be simulated by the following two partial differential equations (PDE) [13,31]:

$$\begin{cases} \kappa \frac{\partial^{2} T}{\partial x^{2}} + \rho H \frac{\partial \alpha}{\partial t} = \rho C_{p} \frac{\partial T}{\partial t} \\ \frac{\partial \alpha}{\partial t} = A exp \left(-\frac{E}{RT} \right) (1 - \alpha)^{n} \alpha^{m} \left[\frac{1}{(1 + exp(C(\alpha - \alpha_{c})))} \right] \end{cases}$$

where T (x, t) is the temperature (K); α % (x,t) represents the curing degree; κ (W m⁻¹ K⁻¹) represents the thermal conductivity; C_p (J kg⁻¹ K⁻¹) is the specific heat; ρ (kg m⁻³) is density; H (J kg⁻¹) is the total enthalpy of the reaction; A is the pre-exponential factor, E is the activation energy, R is the universal gas constant, and R and R are the two orders of reaction constants correlated with the Prout-Tompkins model for autoactivation effects [33]. C and R0 are the constants obtained from literature and experimental results [34]. Another simulation was conducted to understand the effect of nanofillers on the thermal behavior of the frontal curable ink. More details about the simulation can be found in the supporting information.

3. Results and discussion

The collaborative printing of the novolac epoxy resin and its composites are illustrated in Fig. 1 (a). The inks were pneumatically driven through the extrusion nozzle, where the air pressure was set at 5-15 psi depending on the viscosity of the inks. Meanwhile, the ultrasonic nozzle was set at 45-degree against the deposition needle to ensure the effective in-situ mixing of oligomer and curing agents. The heat bed was kept at 90 °C to compensate for the heat dissipation due to the solvent evaporation during the spraying process and to initiate frontal polymerization. The separated storage of ink and curing agent can dramatically improve the pot life of the ink. The mechanism of the frontal reaction is based on the radical-induced cationic polymerization reaction, as shown in Fig. 2 (a). During the frontal polymerization reaction, the thermal labile bonds in I-TI are broken by local heat and generate radicals. Subsequently, the radicals from I-TI induce Lewis acid by interacting with nucleophiles from I-Al for the epoxide ring-opening reaction. Due to the high viscosity of the inks at room temperature, the extruder needs to be heated to improve the flowability of the inks. An empirical viscosity of inks of 10² to 10⁵ mPa.s is recommended for the printing process at a shear rate of about 0.1 s^{-1} [35–37]. Fig. S2 shows the viscosity evolution of novolac epoxy resin from 35 °C to 95 °C [38]. At ambient temperature, the novolac epoxy resin is in a semisolid state and shows an extreme viscosity of $>1 \times 10^6$ mPa.s, which is unsuitable for 3D printing. Some researchers tried to mix novolac epoxy resin with other low viscous resin or a diluent, such as Erisys GE-11, to improve the processability of the novolac epoxy resin [39]. However, this approach typically sacrifices the performance of the novolac epoxy resin [40,41]. With the increase of temperature, the viscosity of the resin decreases significantly. The rheological behavior of the neat resin at 65 °C in various shear rates is illustrated in Fig. 2 (b). When the temperature is set at 65 $^{\circ}$ C, there is no evident shear-thinning phenomenon, but the viscosity reduces a little bit with the increasing shear rate. The inks could flow smoothly from the

nozzle and be deposited on the substrate continuously. The concentric pattern was selected as the printing path because the continuous frontal wave is required during the 3D printing process. A numerical simulation was conducted to predict the relationship between curing degree and printing layer thickness and guide the printing layer thickness selection. The simulated curing distribution along the thickness direction (0.5 mm) is shown in Fig. 2 (c), and the curing degree decreases with increase of the thickness. A self-equilibrium printing strategy was applied to fabricate the specimens. A printing speed window, described in Fig. 2 (d), was estimated based on the fitting curve derived from the frontal velocity at different amplitudes and layer thicknesses from Figs. 3 (a) and 4 (a). Typically, the printing speed should match the rate of the frontal polymerization reaction to ensure the synchronous curing of the thermosets during the manufacturing process. When the printing speed is lower than the frontal velocity, the frontal reaction would selfequilibrate to follow the printing speed due to the low reactivity of the inks [28]. A printing rate <3.5 cm min⁻¹ is preferred when the ultrasonic amplitude is 0.04, and layer thickness < 0.3 mm is desired based on the simulated curing degree distribution. To eliminate the effect of printing speed on the performance of printed samples and provide enough time for solvent evaporation, a printing speed of 3 cm min⁻¹ was selected. The printing accuracy was analyzed by measuring the geometry of the as-printed specimens compared to the original design, as shown in Fig. S3. The dimensions of the geometry were obtained by a caliper and the printed parts show a dimension deviation of around 8.5

3.1. Ultrasonic spraying process

The amplitude of the ultrasonic atomizer could be controlled by the ultrasonic generator. The amplitude describes the severity of the ultrasonic vibration and significantly affects the droplet generation [42]. The effect of amplitudes on the number and the size of spraying droplets was

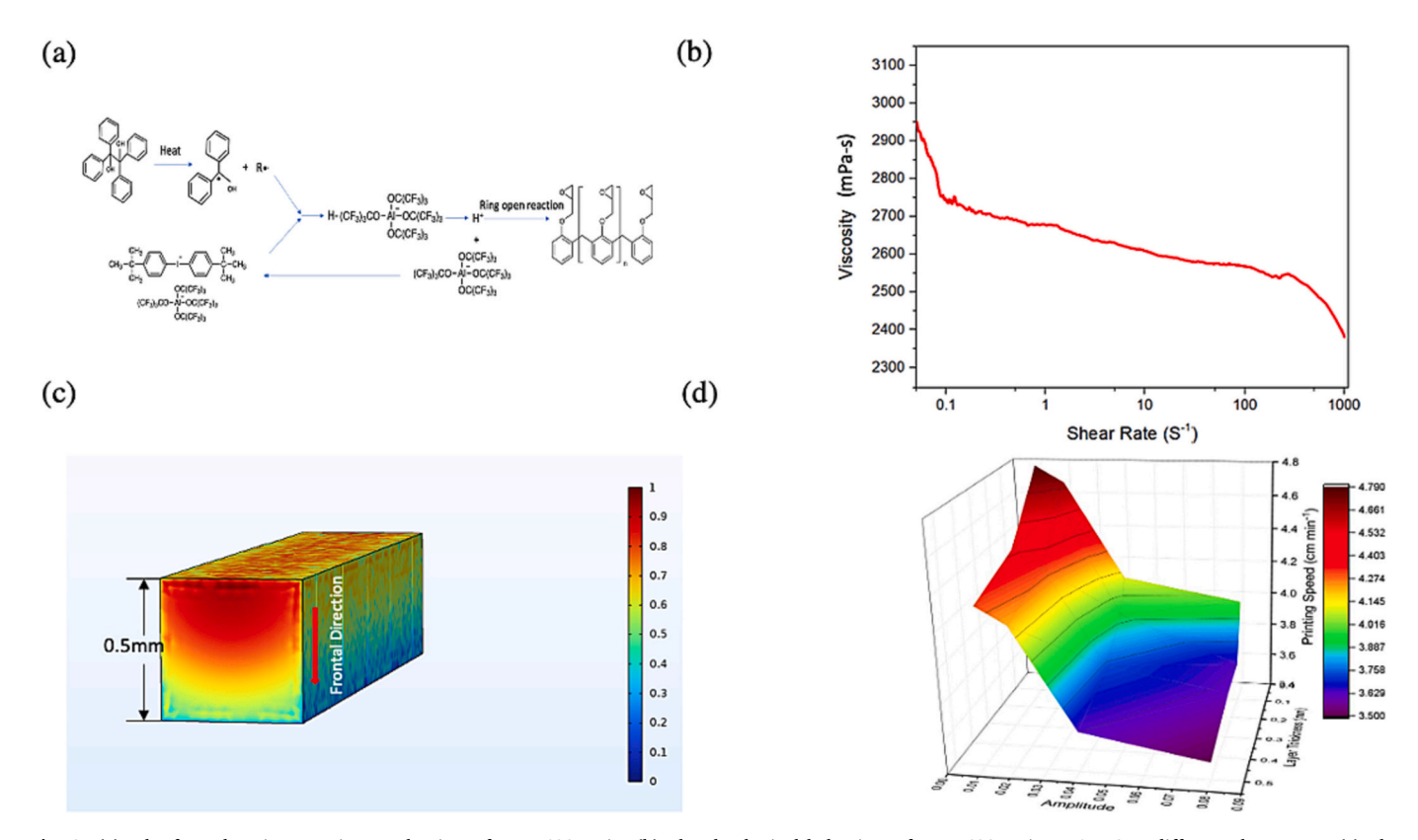


Fig. 2. (a), The frontal curing reaction mechanism of DEN 438 resin, (b) The rheological behaviors of DEN 438 resin at 65 °C at different shear rates, (c) The simulated curing distribution along the thickness direction (1 represents 100 % curing degree), (d) The printing speed window of 3D printing thermosets.

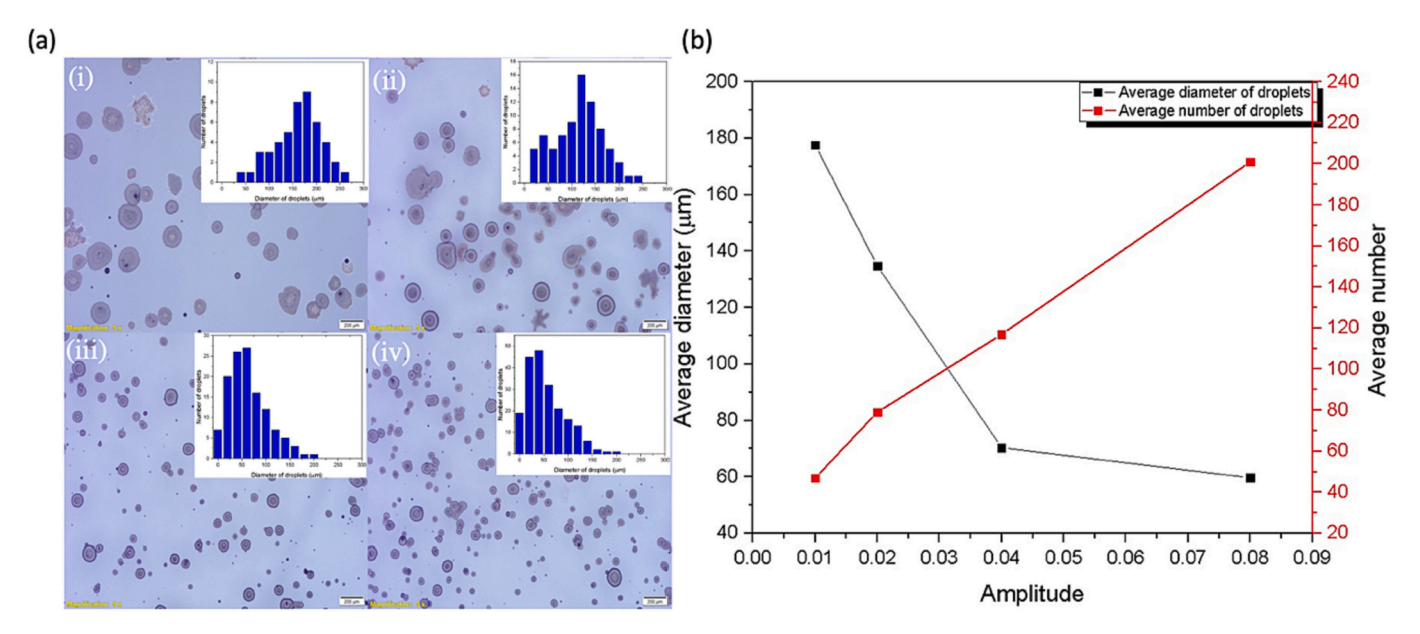


Fig. 3. (a). The optical images of ultrasonic spraying droplets, (i): at 0.01 amplitude; (ii): at 0.02 amplitude; (iii): at 0.04 amplitude; (iv): at 0.08 amplitude, (b) The relationship between the amplitude and droplet size and size distribution.

investigated, and 4 amplitudes, including 0.01, 0.02, 0.04, and 0.08, were tried to spray the curing agent solution. Fig. 3 (a) are the optical microscope images of the ultrasonic spraying curing agent droplets on the glass plate. The image size is 2.5 mm \times 2.5 mm and the spraying time is 0.2 s. The insert pictures in Fig. 3 (a) describe the size distribution of the droplets. The statistical results show that a higher amplitude generates more droplets than a low amplitude because more energy is

applied to overcome the surface tension of the curing agent solution [43]. The number of droplets at 0.01 amplitude is around 47, which is approximately 40 % lower than the number at 0.02 amplitude. The number of droplets increases significantly from about 79 to >200 when the amplitude changes from 0.02 to 0.08, as shown in Fig. 3 (b). The sizes of the ultrasonic spraying droplets show an opposite trend compared to the number of droplets. Fig. 3 (b) gives the diameter

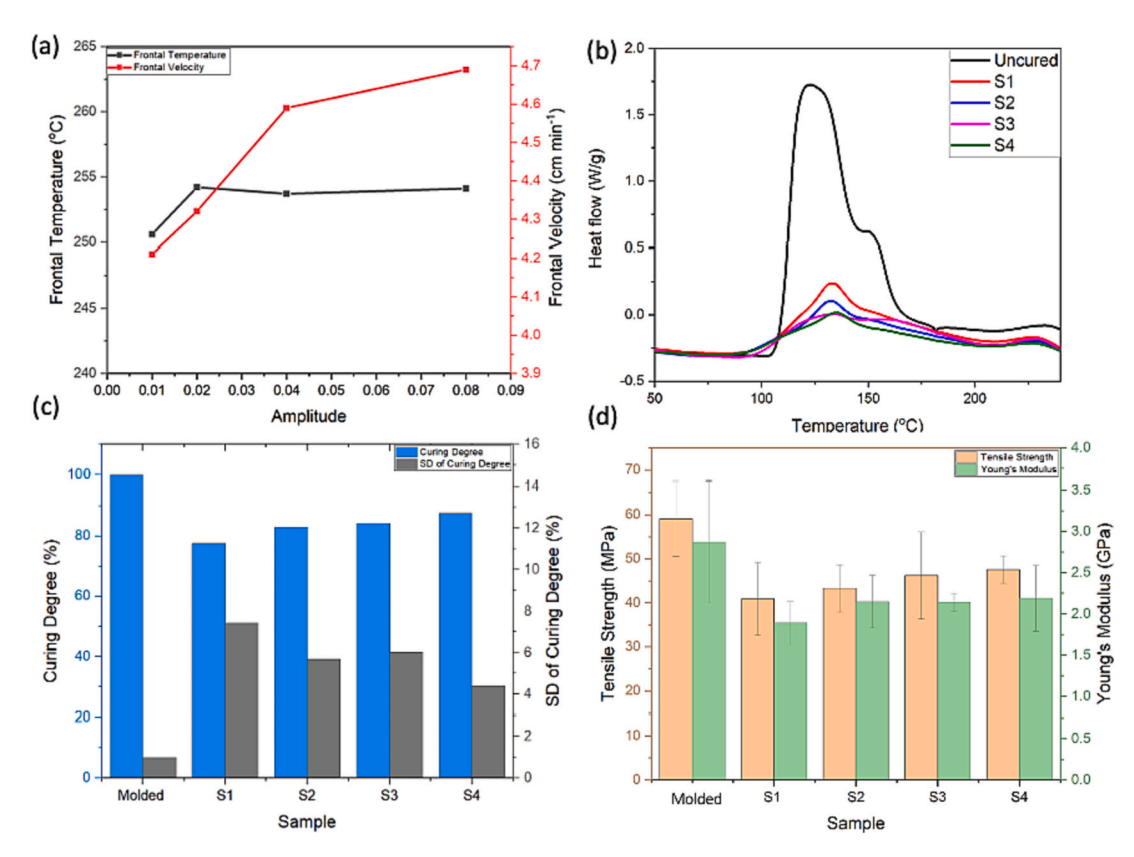


Fig. 4. (a) The effect of amplitudes on frontal temperature and frontal velocity of frontal polymerization reaction, (b) DSC of the printed novolac epoxy resins with different amplitudes (Sample 1–4), (c) The effect of amplitudes on curing degree and curing uniformity, (d) Young's modulus and tensile strength of printed samples and the molded samples.

distribution of the droplets. The figure shows a significant drop in the size of droplets by around 61 %, from 178 to 70 mm when the amplitude increases from 0.01 to 0.04. After that, the decreasing rate of the droplet size becomes lower with the amplitude increasing from 0.04 to 0.08, which shows a similar tendency reported by Manickam [44]. The average size and SD of ultrasonic spraying droplets are shown in Table S1, and more optical images of ultrasonic spraying droplets are presented in Fig. S4. To eliminate the effect of the flow rate of the curing agent solution on the size of the ultrasonic spraying droplets, three different flow rates (0.1 mL/min, 0.25 mL/min, and 1 mL/min) were tried, as presented in Fig. S5, which indicates that the flow rate has no significant influence on the diameter of the curing agent droplets.

3.2. Effect of ultrasonic amplitude

To understand and determine the effect of amplitudes on the frontal curing-assisted 3D printing process, the impact of the amplitude on frontal temperature and frontal velocity was measured first, as shown in Fig. 4(a). The mechanical properties of the printed samples with different ultrasonic amplitudes were examined, and the curing degree and curing uniformity of the as-printed products were measured and analyzed. The tensile specimens (Sample 1-4) were prepared by the same layer thickness (0.1 mm) with different amplitudes (0.01, 0.02, 0.04, 0.08). At the ultrasonic amplitude of 0.01, Sample 1 shows a frontal temperature of 250.6 °C, around 4 °C lower than other samples. There is no apparent variation in the frontal temperature when the ultrasonic amplitude increases from 0.02 to 0.08. That maybe because the droplet numbers keep growing with the amplitudes, and less heat is lost before the front reaches the uncured region. Moreover, the frontal temperature depends on the spraying rate and the resin and initiator ratio. Since all the samples were printed with identical formulation and spraying rate, the frontal temperatures remain similar. The only difference is regarded as the error generated by the IR camera. The frontal velocity increases from around 4.2 to 4.7 cm min⁻¹ when the amplitude increases from 0.01 to 0.08. The curing degrees of the samples were calculated by accumulating the area under the curve in Fig. 4 (b) through the equation presented in 2.4.2. The tensile strength and Young's modulus of the printed and molded samples were measured and compared, as depicted in Fig. 4 (d). In the figure, the tensile strength and Young's modulus of the samples are marked by orange and green colors. The uncured sample reacts enthalpy of 393.9 J/g, while Sample 1 shows a reaction enthalpy of 88.8 J/g with a curing degree of 77.5 %. The molded sample illustrates a tensile strength of around 59 MPa and Young's modulus of about 2.9 GPa, which is 44.4 %, and 51.9 % higher than the data of Sample 1. With the increase of the ultrasonic amplitude, both tensile strength and Young's modulus of the printed samples increase under the same printing layer thickness of 0.1 mm. When the ultrasonic amplitude increases to 0.08, the tensile strength and Young's modulus reach 47.56 MPa and 2.19 GPa, which is a 16.3 % and 15.9 % improvement compared with Sample 1. This is because a higher ultrasonic amplitude would generate smaller size and more significant number of curing agent droplets, further improving the curing degree of printed samples. The curing degree of Sample 4 is around 87.5 % which is 10 % higher than Sample 1. However, the curing degree of the molded sample is 99.3 %, resulting from a better dispersion of the curing agent in the resin and a more uniform curing reaction. The curing variation resulting from the different sizes and numbers of the curing agent droplets generated by ultrasonic amplitudes is characterized by the SD of the curing degree, as shown in Fig. 4(c). When the amplitude is 0.01, the SD of the curing degree for Sample 1 is 7.45 %, the highest value among the 4 values. As the amplitude increases, the SD of the curing degree exhibits a reducing trend though Sample 3 has a slightly higher value than Sample 2. According to the results above, a higher amplitude is applied, and a more uniformly cured sample is obtained.

3.3. Effect of printing layer thickness

The effect of the printing layer thicknesses on frontal polymerization was investigated then. The printing layer thicknesses were set at 0.05, 0.1, 0.25, and 0.5 mm, and 0.08 ultrasonic amplitude was selected for all the samples (Sample 4 shares the same parameters as Sample 6). The frontal temperature of Sample 5 is 253.6 °C which is close to Sample 6, and Sample 7 and 8 show a similar frontal temperature at around 250 °C, as shown in Fig. 5(a). This is consistent with the frontal temperature obtained in Sample 1. The frontal velocity decreases with the rise of layer thickness. The lowest frontal velocity is 3.98 cm min⁻¹ with a layer thickness of 0.5 mm. The DSC data presented in Fig. 5 (b) were used to calculate the curing degrees of printed samples. Fig. 5 (c) gives the average curing degree and SD of the curing degree. Sample 5 demonstrates a reaction enthalpy of 42.54 J/g and has the highest curing degree of 89.2 %, with the smallest SD of curing degree at 3.91 % among the 8 printed samples. Obviously, the curing degree decreases with the augment of the printing layer thickness. Interestingly, the span of the curing degree of Sample 5-8 is almost 20 %, which is twice more prominent than that of Sample 1-4. Sample 8 has the lowest curing degree at 70.7 % and the highest SD of curing degree at 14.77 %, showing a more considerable curing uniformity variation generated by other smaller printing layer thicknesses. Compared to Sample 1-4, the SD of curing degree of Sample 5-8 varies from 3.91 % to 14.77 %, resulting from the significant change in the printing layer thickness. These results demonstrate that the printing layer thickness plays a more critical role in curing uniformity than the ultrasonic amplitude. The tensile strength and Young's modulus of Sample 5-8 also show a reducing tendency while the printing layer thickness keeps increasing, as shown in Fig. 5 (d). This is attributed to a more completed polymer network forming when a higher curing degree of the sample is achieved, and higher tensile strength is obtained. The tensile strength and Young's modulus of Sample 5 are 47.73 MPa, almost the same as Sample 6, and 2.26 GPa, which is only a 3.2 % improvement from Sample 6. The lowest tensile strength and Young's moduli are 37.9 MPa and 1.72 GPa from Sample 8. The values decrease significantly by 9.83 MPa and 0.54 GPa, respectively.

3.4. Printing of thermoset composites

To demonstrate the feasibility of additive manufacturing of thermoset composites, d-CF and glass microballoon were applied to manufacture reinforced composites. The rheological behaviors of d-CF and microballoon-filled inks were characterized to check the printability of the inks, as shown in Fig. 6 (a). 1 wt%, 3 wt%, and 5 wt% d-CF were mixed with epoxy ink, and only 1 wt% microballoon was tried because of the dispersion issue of the glass nanosphere. Fig. S6 shows the optical images of the composite inks and indicates a good dispersion of fillers in inks. Adding d-CF increases the viscosity of the inks, and there is no noticeable shear-thinning behavior of the 1 wt%, 3 wt% d-CF, and 1 wt% microballoon ink. However, when the d-CF concentration reached 5 wt %, an assertive shear-shinning behavior was observed, resulting from forming a transient, interconnected 3D network of fibers in the presence of the external shear. The viscous inks were dispensed and deposited on the heated printing bed to initiate the frontal polymerization. The novolac epoxy resins with 1 wt%, 3 wt%, 5 wt% d-CF, and 1 wt% microballoon are marked as Sample 9, 10, 11, and 12, respectively. The printing parameters of the composite samples are listed in Table 2, and the frontal velocity of the composite ink is provided in Fig. S7. The effects of the d-CF and microballoon on the curing degree, curing uniformity, and mechanical property of the printed composites were measured and analyzed. The curing degrees of the printed samples were calculated by the DSC data, as shown in Fig. 6 (b). The strain-stress curve of the printed thermoset composites are shown in Fig. 6 (c), and the tensile strength and Young's modulus of the samples are presented in Fig. 6 (d). Sample 12 (1 wt% microballoon DEN 438) shows a curing

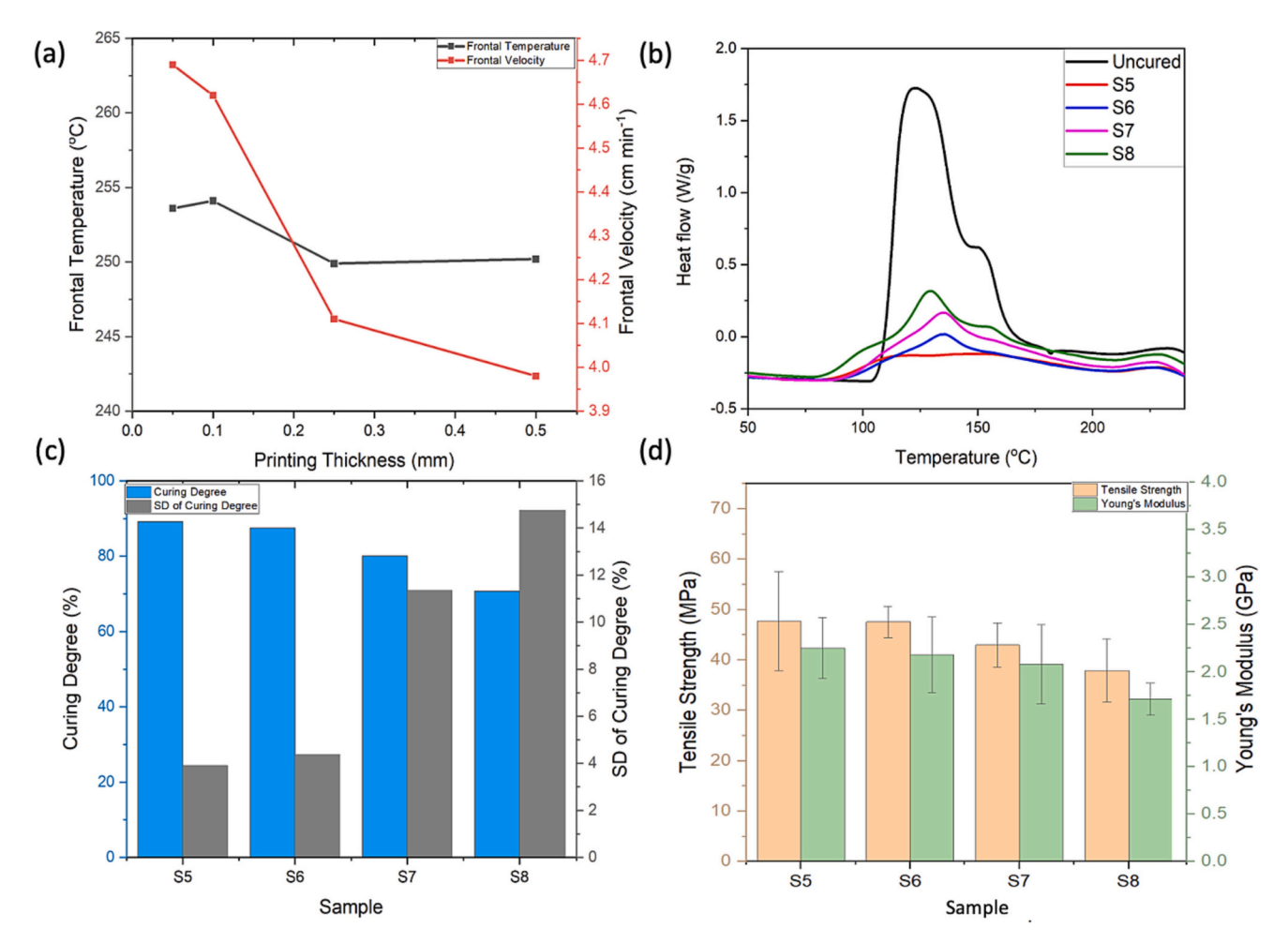


Fig. 5. (a) The effect of layer thickness on frontal temperature and frontal velocity of frontal polymerization reaction, (b) DSC of printed novolac epoxy resin with different layer thickness (Sample 5–8), (c), The effect of printing layer thickness on curing degree and curing uniformity, (d) Tensile strength, and Young's modulus of the printed samples.

degree of 86.3 %, slightly lower than the value of neat resin, and the SD of the curing degree is around 6.9, which is also higher than the neat resin, whose value is approximately 4.4. This maybe because the glass nanosphere slows the heat transfer inside the frontal curable ink [45]. For the mechanical property, both tensile strength and Young's modulus are lower than the CF-epoxy thermosets. This should be attributed to the microballoon composites' low curing degree caused by their low thermal conductivity and the geometry of the nanosphere [46]. With the addition of the d-CF, the frontal temperature, curing degree, tensile strength, and Young's modulus of the composites keep increasing slightly at a rate of 5 % until the concentration of the CF reaches 5 wt%. The high amount of CF would be highly aligned with the shear forces along the printing direction. As a result, the tensile strength and Young's modulus of Sample 11 are 66.71 MPa and 3.65 GPa, which is about 26.4 % and 55.6 % improvement from Sample 10 where the CF is randomly distributed [28]. The curing degree of Sample 11 is 92.1 %, which is 1.1 % smaller than Sample 10. This may contribute to the fact that a higher amount of d-CF (5 wt%) enhances heat dissipation during the frontal polymerization process and further reduce the curing degree of Sample 11. The overall curing uniformity of the d-CF-filled composites is around 4.64 % which is lower than that of the microballoon-filled samples. Sample 12 shows an SD of curing degree at 6.94, which is even higher than the neat epoxy resin because of the low heat transfer efficiency of the microballoon-filled ink [47]. The simulated results show the temperature profiles along the thickness direction, as shown in Fig. S8 (a), where i represents the 1 wt% microsphere-filled composites, ii means the neat resin, and iii is the 1 wt% d-CF-filled composites. The layer thickness was set at 0.1 mm. The temperature profiles on the spraying surface are shown in Fig. S8 (b). Fig. S8 (a) and (b) show that the d-CF can enhance heat transfer in the frontal polymerization direction because of its excellent thermal conductivity. Therefore, the temperature profile of 1 wt% d-CF-epoxy is a little sharper than that of the neat resin and can reach a higher temperature at around 257 °C. The results show a similar trend with the frontal curing assisted 3D printing continuous carbon fiber (c-CF) reinforced thermosets but not as sharp as the c-CF one due to the heat transfer efficiency between the c-CF and d-CF [29]. A blunt temperature gradient was observed for the neat resin, and the final frontal temperature is 5 °C lower than the CF one, which is confirmed by the experimental results. 1 wt% microballoon-epoxy had the lowest final temperature with the longest time to get it in comparison with the other two curves, as shown in Fig. S8 (a). This is due to the low thermal conductivity of the glass sphere.

4. Conclusion

In this study, a novel additive manufacturing method for printing and in-situ frontal curing of highly-viscous thermosets and composites was reported. The frontal curing agent solution was sprayed by the ultrasonic atomizer to achieve an in-situ mixing with the resin oligomers at a microscale level. The effect of the ultrasonic amplitude and printing layer thickness on the frontal temperature and frontal velocity of the frontal polymerization reaction were investigated. The curing degree,

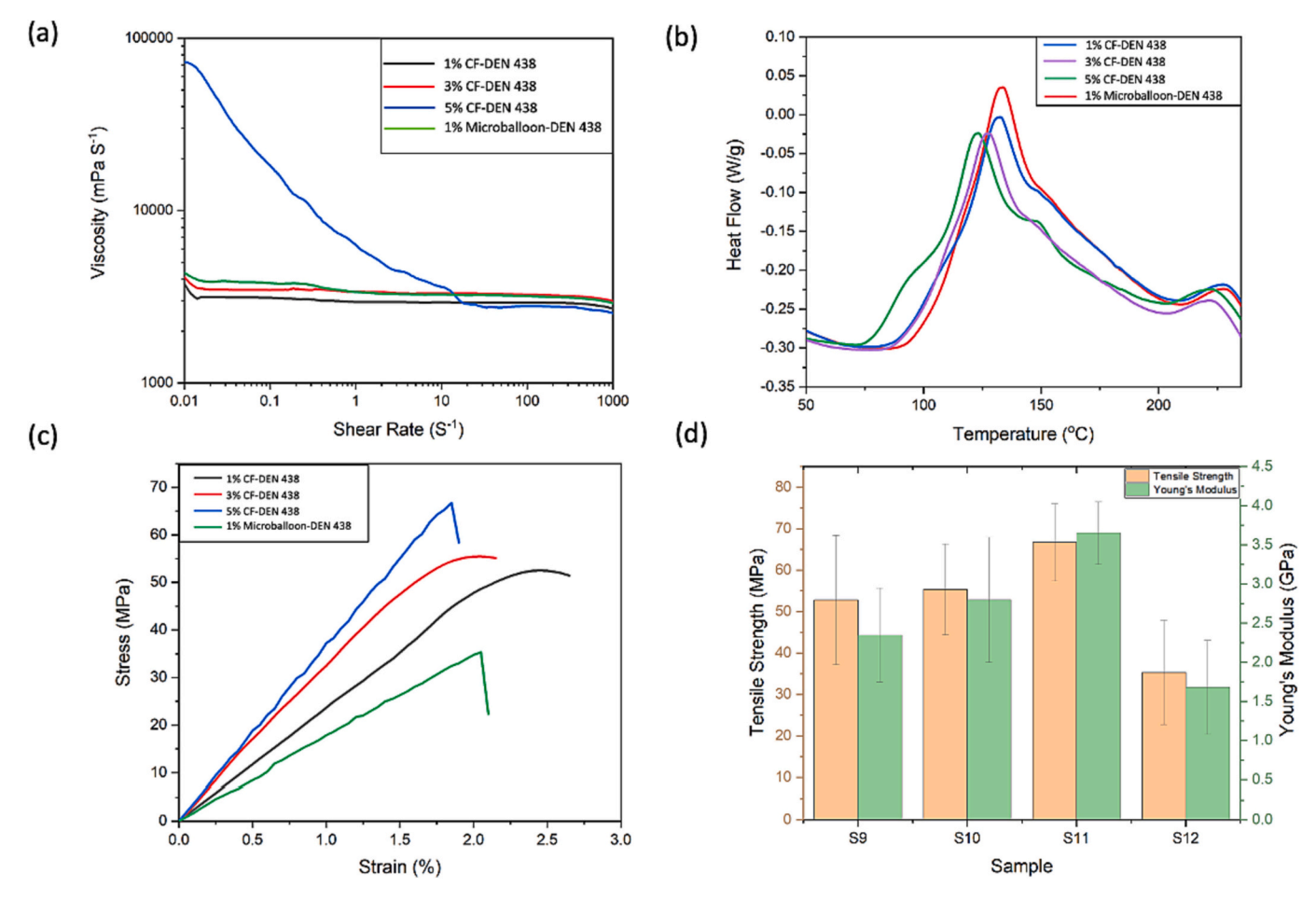


Fig. 6. (a). The rheological behaviors of composite ink of 65 °C at different shear rates. (b) DSC data of 3D printed composite samples (c) Strain-stress curve of the 3D printed samples (d) Tensile strength and Young's modulus of the 3D printed composite samples.

Table 2 Printed composite samples.

Sample number	Ultrasonic amplitude	Layer thickness (mm)	Filler	Frontal temperature (°C)	Degree of cure (%)	SD of curing degree (%)
S9	0.08	0.1	1 wt% d-CF	254.8	87.9	4.62
S10	0.08	0.1	3 wt% d-CF	257.5	93.2	5.06
S11	0.08	0.1	5 wt% d-CF	255.3	92.1	4.24
S12	0.08	0.1	1wt%microballoon	250.3	86.3	6.94

curing uniformity, and mechanical property of printed samples were measured and analyzed. From our results, the frontal velocity improves with the rise of the ultrasonic amplitude, and decreases with the increase of the layer thickness. When the ultrasonic amplitude increases to 0.08, the tensile strength and Young's modulus reach 47.56 MPa and 2.19 GPa. Sample 5 demonstrates a reaction enthalpy of 42.54 J/g and has the highest curing degree of 89.2 %, with the smallest SD of curing degree at 3.91 among the 8 printed neat resin samples. The curing degree decreases with the augment of the printing layer thickness, and the printing layer thickness plays a more critical role in curing uniformity than the ultrasonic amplitude. The application of this printing method for composite manufacturing was demonstrated. d-CF and microballoon were used as the fillers, and the performance of the printed composites was characterized. When the d-CF concentration was 1 wt%, the composites showed a tensile strength and Young's Modulus of 52.78 MPa and 2.35 GPa.

The highest tensile strength and Young's modulus of 66.71 MPa and 3.65 GPa were achieved with 5 wt% loading of d-CF. Further research needs to modify the d-CF and glass microsphere to improve the

nanofillers' dispersion and enhance the mechanical performance of the composites.

Author contributions

S.W. conceived the research; S. W., C.G., and R. L. designed the experiments. C. G., R. L., and W.L. prepared samples and measured the properties. C.G., R.L., W.L., J. Q., and S.W. analyzed the data and wrote the manuscript with comments and inputs from all authors.

Declaration of competing interest

There is no conflict of interest regarding this research.

Data availability

All the data in this work is available upon request.

Acknowledgments

We appreciate the funding support from National Science Foundation (CMMI-1934120, CMMI-1933679).

Appendix A. Supplementary data

Supplementary data to this article can be found online at https://doi.org/10.1016/j.jmapro.2023.01.048.

References

- [1] C Gao J Qiu S. Wang In-situ curing of 3D printed freestanding thermosets. J Adv Manuf Processe10114. doi: doi:10.1002/amp2.10114.
- [2] Tamez MBA, Taha I. A review of additive manufacturing technologies and markets for thermosetting resins and their potential for carbon fiber integration. Addit Manuf 2021;37:101748. https://doi.org/10.1016/j.addma.2020.101748.
- [3] Duty C, Ajinjeru C, Kishore V, Compton B, Hmeidat N, Chen X, et al. What makes a material printable? A viscoelastic model for extrusion-based 3D printing of polymers. J Manuf Process 2018;35:526–37. https://doi.org/10.1016/j. imapro.2018.08.008.
- [4] Manning KB, Wyatt N, Hughes L, Cook A, Giron NH, Martinez E, et al. Self assembly-assisted additive manufacturing: direct ink write 3D printing of epoxy-amine thermosets. Macromol Mater Eng 2019;304(3):1800511. https://doi. org/10.1002/mame.201800511.
- [5] Nawafleh N, Celik E. Additive manufacturing of short fiber reinforced thermoset composites with unprecedented mechanical performance. Addit Manuf 2020;33: 101109. https://doi.org/10.1016/j.addma.2020.101109.
- [6] Timmis AJ, Hodzic A, Koh L, Bonner M, Soutis C, Schäfer AW, et al. Environmental impact assessment of aviation emission reduction through the implementation of composite materials. Int J Life Cycle Assess 2015;20(2):233–43. https://doi.org/ 10.1007/s11367-014-0824-0
- [7] Wang B, Zhang Z, Pei Z, Qiu J, Wang S. Current progress on the 3D printing of thermosets. Adv Compos Hybrid Mater 2020;3(4):462–72. https://doi.org/ 10.1007/s42114-020-00183-z.
- [8] Odom MG, Sweeney CB, Parviz D, Sill LP, Saed MA, Green MJ. Rapid curing and additive manufacturing of thermoset systems using scanning microwave heating of carbon nanotube/epoxy composites. Carbon 2017;120:447–53. https://doi.org/ 10.1016/j.carbon.2017.05.063.
- [9] Wiese M, Thiede S, Herrmann C. Rapid manufacturing of automotive polymer series parts: a systematic review of processes, materials and challenges. Addit Manuf 2020;36:101582. https://doi.org/10.1016/j.addma.2020.101582.
- [10] Evans RS, Bourell DL, Beaman JJ, Campbell MI. Rapid manufacturing of silicon carbide composites. Rapid Prototyp J 2005. https://doi.org/10.1108/ 13552540510573374
- [11] Lei D, Yang Y, Liu Z, Chen S, Song B, Shen A, et al. A general strategy of 3D printing thermosets for diverse applications. Mater Horiz 2019;6(2):394–404. https://doi. org/10.1039/C8MH00937F.
- [12] Zhang Z, Gao C, Liu R, Qiu J, Pei ZZ, Wang S. 3D printing of frontal-polymerized multiscale epoxy thermoset and composites. Manuf Lett 2022;33:640–3. https://doi.org/10.1016/j.mfglet.2022.07.079.
- [13] Robertson ID, Yourdkhani M, Centellas PJ, Aw JE, Ivanoff DG, Goli E, et al. Rapid energy-efficient manufacturing of polymers and composites via frontal polymerization. Nature 2018;557(7704):223–7.
- [14] Wang B, Arias KF, Zhang Z, Liu Y, Jiang Z, Sue H-J, et al. 3D printing of in-situ curing thermally insulated thermosets. Manuf Lett 2019;21:1–6. https://doi.org/ 10.1016/j.mfglet.2019.06.001.
- [15] Zhang Z, Gao C, Liu R, Li W, Qiu J, Wang S. Catalyzed frontal polymerization-aided 3D printing of epoxy thermosets. Addit Manuf Lett 2022:100030. https://doi.org/ 10.1016/j.addlet.2022.100030.
- [16] Uitz O, Koirala P, Tehrani M, Seepersad CC. Fast, low-energy additive manufacturing of isotropic parts via reactive extrusion. Addit Manuf 2021;41: 101919. https://doi.org/10.1016/j.addma.2021.101919.
- [17] Zhang Z, Liu R, Li W, Liu Y, Pei Z, Qiu J, et al. Frontal polymerization-assisted 3D printing of short carbon fibers/dicyclopentadiene composites. J Manuf Process 2021;71:753–62. https://doi.org/10.1016/j.imapro.2021.10.014.
- [18] Yuan S, Li S, Zhu J, Tang Y. Additive manufacturing of polymeric composites from material processing to structural design. Compos Part B Eng 2021;219:108903. https://doi.org/10.1016/j.compositesb.2021.108903.
- [19] Bonada J, Muguruza A, Fernández-Francos X, Ramis X. Influence of exposure time on mechanical properties and photocuring conversion ratios for photosensitive materials used in additive manufacturing. Procedia Manuf 2017;13:762–9. https:// doi.org/10.1016/j.promfg.2017.09.182.
- [20] Ligon SC, Liska R, Stampfl J, Gurr M, Mülhaupt R. Polymers for 3D printing and customized additive manufacturing. Chem Rev 2017;117(15):10212–90. https:// doi.org/10.1021/acs.chemrev.7b00074.

- [21] Seraji SM, Gan H, Issazadeh S, Varley RJ. Investigation of the dual polymerization of rapid curing organophosphorous modified epoxy/amine resins and subsequent flame retardancy. Macromol Chem Phys 2021;222(7):2000342. https://doi.org/ 10.1002/macp.202000342.
- [22] Schmidt C, Ciesielski M, Greiner L, Döring M. Novel organophosphorus flame retardants and their synergistic application in novolac epoxy resin. Polym Degrad Stab 2018;158:190–201. https://doi.org/10.1016/j. polymdegradstab.2018.09.001.
- [23] Rajagopalan N, Weinell CE, Dam-Johansen K, Kiil S. Degradation mechanisms of amine-cured epoxy novolac and bisphenol F resins under conditions of high pressures and high temperatures. Prog Org Coat 2021;156:106268. https://doi. org/10.1016/j.porgcoat.2021.106268.
- [24] Rau DA, Forgiarini M, Williams CB. Hybridizing direct ink write and mask-projection vat photopolymerization to enable additive manufacturing of high viscosity photopolymer resins. Addit Manuf 2021;42:101996.
- [25] Gunduz J, McClain M, Cattani P, Chiu G-C, Rhoads J, Son S. 3D printing of extremely viscous materials using ultrasonic vibrations. Addit Manuf 2018;22: 98–103. https://doi.org/10.1016/j.addma.2018.04.029.
- [26] Liu Z, Pan W, Wang K, Matia Y, Xu A, Barreiros JA, et al. Acoustophoretic liquefaction for 3D printing ultrahigh-viscosity nanoparticle suspensions. Adv Mater 2022;34(7):2106183. https://doi.org/10.1002/adma.202106183.
- [27] Frulloni E, Salinas M, Torre L, Mariani A, Kenny JM. Numerical modeling and experimental study of the frontal polymerization of the diglycidyl ether of bisphenol A/diethylenetriamine epoxy system. J Appl Polym Sci 2005;96(5): 1756–66. https://doi.org/10.1002/app.21644.
- [28] Ziaee M, Johnson JW, Yourdkhani M. 3D printing of short-carbon-fiber-reinforced thermoset polymer composites via frontal polymerization. ACS Appl Mater Interfaces 2022;14(14):16694–702. https://doi.org/10.1021/acsami.2c02076.
- [29] Zhang Z, Liu R, Li W, Liu Y, Luo H, Zeng L, et al. Direct writing of continuous carbon fibers/epoxy thermoset composites with high-strength and low energyconsumption. Addit Manuf 2021;47:102348.
- [31] Goli E, Parikh N, Yourdkhani M, Hibbard N, Moore J, Sottos N, et al. Frontal polymerization of unidirectional carbon-fiber-reinforced composites. Compos A: Appl Sci Manuf 2020;130:105689.
- [32] Pojman JA, Ilyashenko VM, Khan AM. Free-radical frontal polymerization: self-propagating thermal reaction waves. J Chem Soc Faraday Trans 1996;92(16): 2825–37. https://doi.org/10.1039/FT9969202825.
- [33] Goli E, Robertson ID, Geubelle PH, Moore JS. Frontal polymerization of dicyclopentadiene: a numerical study. J Phys Chem B 2018;122(16):4583–91.
- [34] Goli E, Peterson SR, Geubelle PH. Instabilities driven by frontal polymerization in thermosetting polymers and composites. Compos Part B Eng 2020;199:108306. https://doi.org/10.1016/j.compositesb.2020.108306.
- [35] Tagliaferri S, Panagiotopoulos A, Mattevi C. Direct ink writing of energy materials. Mater Adv 2021;2(2):540–63. https://doi.org/10.1039/D0MA00753F.
- [36] Saadi M, Maguire A, Pottackal NT, Thakur MSH, Ikram MM, Hart AJ, et al. Direct ink writing: a 3D printing technology for diverse materials. Adv Mater 2022: 2108855. https://doi.org/10.1002/adma.202108855.
- [37] Li X, Zhang P, Li Q, Wang H, Yang C. Direct-ink-write printing of hydrogels using dilute inks. Iscience 2021;24(4):102319. https://doi.org/10.1016/j. isci.2021.102319.
- [38] Pham HQ, Marks MJ. Epoxy resins. In: Ullmann's encyclopedia of industrial chemistry: 2000.
- [39] Campanella A, La Scala JJ, Wool RP. The use of acrylated fatty acid methyl esters as styrene replacements in triglyceride-based thermosetting polymers. Polym Eng Sci 2009;49(12):2384–92. https://doi.org/10.1002/pen.21486.
- [40] Martin C, Lligadas G, Ronda J, Galia M, Cadiz V. Synthesis of novel boron-containing epoxy–novolac resins and properties of cured products. J Polym Sci A Polym Chem 2006;44(21):6332–44. https://doi.org/10.1002/pola.21726.
- [41] Vanaja A, Rao R. Synthesis and characterisation of epoxy-novolac/bismaleimide networks. Eur Polym J 2002;38(1):187-93. https://doi.org/10.1016/S0014-3057 (01)00094-5.
- [42] Zhu P, Tang X, Wang L. Droplet generation in co-flow microfluidic channels with vibration. Microfluid Nanofluid 2016;20(3):1–10. https://doi.org/10.1007/ s10404-016-1717-2.
- [43] Sugondo A, Anggono W, Anne O. Effect of frequency on droplet characteristics in ultrasonic atomization process. E3S Web Conf EDP Sci 2019:01002.
- [44] Manickam S, Sivakumar K, Pang CH. Investigations on the generation of oil-in-water (O/W) nanoemulsions through the combination of ultrasound and microchannel. Ultrason Sonochem 2020;69:105258. https://doi.org/10.1016/j.ultsanch.2020.105258
- [45] Vyas S, Goli E, Zhang X, Geubelle P. Manufacturing of unidirectional glass-fiber-reinforced composites via frontal polymerization: a numerical study. Compos Sci Technol 2019;184:107832. https://doi.org/10.1016/j.compscitech.2019.107832.
- [46] Spoerk M, Savandaiah C, Arbeiter F, Sapkota J, Holzer C. Optimization of mechanical properties of glass-spheres-filled polypropylene composites for extrusion-based additive manufacturing. Polym Compos 2019;40(2):638–51 https://doi.org/10.1002/pc.24701.
- [47] Tian Q, Yu D. Preparation and properties of polymer microspheres filled epoxy composite films by UV-curable polymerization. Mater Des 2016;107:221–9. https://doi.org/10.1016/j.matdes.2016.06.035.